Non-rigid Registration of Mammograms Obtained with Variable Breast Compression: A Phantom Study

Frédéric J.P. Richard[1], Predrag R. Bakić[2], and Andrew D.A. Maidment[2]

[1] MAP5, FRE CNRS 2428, University Paris 5 - René Descartes
Department of Mathematics and Computer Science
45, rue des Saints Pères, 75270 Paris Cedex 06, France
richard@math-info.univ-paris5.fr
[2] Hospital of the University of Pennsylvania
Department of Radiology, 1 Silverstein Bldg
3400 Spruce St., Philadelphia, PA 19104, USA
{bakic,maidment}@rad.upenn.edu

Abstract. The amount of breast compression applied during a mammographic exam affects the appearance of mammograms by introducing variations in the shape, position, and contrast of breast anatomical structures, which can conceal existing breast abnormalities or generate false alarms. Due to the complex tissue organization and elastic properties of the breast and the projective nature of mammography, rigid registration approaches are not useful in correcting these variations. We describe a non-rigid approach focused on registration of mammogram regions of interest, taking into account the changes in image contrast. This registration algorithm has been applied to synthetic mammograms generated using a deformable 3D anthropomorphic phantom and a model of breast deformation during mammographic compression.

Keywords: image registration, partial differential equations, multigrid optimization, finite elements, multimodality registration, mammography, breast compression, tissue modeling, mammogram synthesis.

1 Introduction

Image registration has been an active topic of research for over a decade (see [1] for a recent survey). The most common medical application is in brain imaging [2, 3]. Although less studied, mammogram registration is not only a challenging problem but also an important issue for computer-aided diagnosis. One of the main approaches to tumor detection consists of locally comparing mammograms and identifying abnormal differences [4–8]. This approach can be applied either to successive mammograms of the same breast or mammograms of both the left and right breasts. In the first case, abnormal differences are a sign of possible lesion growth, whereas in the second case they are a sign of suspicious asymmetry. Unfortunately, such comparisons lack specificity due to the large number of normal mammogram differences which are locally similar to abnormalities and cause false-positives.

The main problem in the design of a robust comparison technique is to reduce false-positives by recognizing normal mammogram differences. Normal differences can be

J.C. Gee et al. (Eds.): WBIR 2003, LNCS 2717, pp. 281–290, 2003.

due to several factors: acquisition differences, breast positioning and compression variations, and anatomical or histological variations. Differences resulting from acquisition conditions are often very prominent in successive mammograms. They can be corrected by mammogram grey-scale normalization [9]. Differences due to breast positioning can be easily corrected by alignment procedures which involve rotation and translation computed using breast contours [8]. But, the correction of differences due to the last three factors (compression and histological and anatomical variations) is still an open problem. The effect of these factors on a mammogram are not well-known. Modeling mammographic compression effects is an important recent topic of research [10, 11, 9, 12]. Non-rigid image registration techniques have been proposed to correct image differences that remain after mammogram normalization and alignment [4, 5, 7]. However, none of these works has systematically evaluated the ability of techniques to correct each type of difference. Such evaluations are difficult to implement because they require very specific mammogram databases that are not available in the public domain.

Our motivation is to automatically correct mammogram differences due to breast compression variations. Our main contribution is two fold. First, based upon recent works of F. Richard and L. Cohen [4, 5], we propose a new image registration technique which enables such corrections. Second, we show preliminary results of an evaluation based upon synthetic mammograms simulated with a deformable breast phantom [12, 13]. Here we present a report of our work in progress.

In [4, 5], F. Richard and L. Cohen proposed an image-matching approach that focuses on regions of interest. This approach allows a combination of constraints which are intensity and contour based. Such a combination is well-suited for mammogram registration. Breast contours are the most widely used constraint for registration, as they provide robust corrections of breast shape differences. However, these constraints are not sufficient to register accurately changes in internal breast anatomy. Such registrations can be obtained by completing models with some other constraints based on image intensity. In [4, 5], intensity-based constraints are defined using the mean square distance (MSD) between image grey levels (see section 2.1). This similarity measure is generally used in registration of images from a single modality and is well-suited for cases where grey levels are approximately the same from one image to another. Large variations of breast compression can, however, significantly change image contrast. In order to overcome this limitation, we have modified the registration approach allowing linear change of image contrast, similarly to the registration of multimodality images [14, 15]. This modified approach, however, differs by enabling non-rigid deformations, while still combining intensity-based with contour-based constraints. In Section 2, we describe this new registration approach. In Section 3, we present the model which is used to simulate mammograms of a breast with different amounts of compression. In Section 4, we show some registration experiments using simulated mammograms.

2 Registration Technique

2.1 Framework

Let Ω be a connected and open set of $\mathbb{R}^2$ and I^0 and I^1 be two images defined on Ω using interpolation. Let us denote by $\overline{\Omega}$ the set which is the closure of Ω (with

respect to the Euclidean norm of $\mathbb{R}^2$), i.e., the set which contains the set Ω and its boundary. Matching images I^0 and I^1 consists of finding a geometric deformation ϕ such that the deformed image $I^0 \circ \phi$ is "similar" to the target image I^1. Usually [16–18], images are registered on the whole domain Ω and geometric deformations are defined as functions mapping Ω onto itself. As in [4, 5], we focus rather on mapping image regions of interest. For that, we assume that images I^0 and I^1 have single regions of interest which are respectively located on the connected and open subsets Ω_0 and Ω_1 of Ω. We denote by $\partial\Omega_0$ and $\partial\Omega_1$ the boundaries of Ω_0 and Ω_1, respectively. In the registration model defined next, boundaries $\partial\Omega_1$ in I^1 are assumed to be segmented and known whereas boundaries $\partial\Omega_0$ are unknown and segmented during the registration process. We define geometric deformations ϕ on the known region of interest $\overline{\Omega_1}$ of I^1. These deformations are elements of a space $\mathcal{W}$ which is composed of smooth functions mapping the domain $\overline{\Omega_1}$ into $\overline{\Omega}$. We will denote by u a displacement fields associated with deformations ϕ. Displacements u also belong to $\mathcal{W}$. They are equal to $\phi - \mathrm{Id}$, where Id is the identity map of $\mathcal{W}$ (i.e. $\forall\, x \in \overline{\Omega}, \mathrm{Id}(x) = x$).

In registration tasks involving a single modality, the image similarity criterion is usually the MSD. For all images I^0 and I^1 in $L^2(\Omega)$ and any open subset U of Ω, this distance is defined as:

$$D_U^2(I^0, I^1) = |I^0 - I^1|_U^2 = \int_U (I^0(x) - I^1(x))^2 \, dx. \tag{1}$$

This distance is low if on each point of U, grey levels values of both images I^0 and I^1 are close. This distance is not invariant with contrast changes. Hence, a MSD criterion is not suitable for the similarity quantification of images having different contrasts. One of the ways to define a criterion $D_{U,\mathcal{C}}$ which is invariant to a group $\mathcal{C}$ of contrast changes is the following:

$$D_{U,\mathcal{C}}^2(I^0, I^1) = \inf_{g \in \mathcal{C}} |g \cdot I^0 - I^1|_U^2. \tag{2}$$

In this definition, $g \cdot I^0$ is the action of a contrast change g of $\mathcal{C}$ on I^0. In this paper, we will simply use a measure which is invariant to linear contrast changes. Hence, in what follows, the set $\mathcal{C}$ will be equal to $\mathbb{R}^2$ and the action of an element $g = (g_1, g_2)$ of $\mathcal{C}$ on an image I will be defined as

$$g \cdot I = g_1 \, I + g_2. \tag{3}$$

In this equation, g_1 is a grey-level dilatation factor and g_2 is a translation factor. Let ϕ be in $\mathcal{W}$ and g in $\mathcal{C}$, we will denote by $I_{\phi,g}$ the geometric deformation of the image I under the contrast change g:

$$\forall\, x \in \Omega_1, \;\; I_{\phi,g}(x) = g \cdot I \circ \phi(x) = g_1 \, I(\phi(x)) + g_2. \tag{4}$$

When $g = (1, 0)$, $I_{\phi,g}$ will be also denoted I_ϕ.

2.2 Mathematical Model

The registration problem is stated in terms of an inverse problem as follows:
Problem 1 (first formulation) *Find an element of $\mathcal{W}$ which minimizes an energy $\tilde{J}$ of the following form:*

$$\tilde{J}(u) = \frac{1}{2}\, A_{\Omega_1}(u,u) + \frac{\gamma_1}{2}\, D^2_{\Omega_1,\mathcal{C}}(I^0_\phi, I^1) + \gamma_2 \int_{\Omega - \phi(\Omega_1)} S((I^0(x))^2) dx, \quad (5)$$

with free boundary conditions on $\partial\Omega_1$. In this energy definition, parameters γ_1 and γ_2 both belong to $\mathbb{R}^+$.

The energy in Equation (5) is composed of three terms. The first term is a smoothing term which ensures that the problem is well-posed and that solutions are non-degenerate. As in [5, 4], the design is based on a strain energy of the linearized elasticity. The second term is the image similarity measure defined in Equation (2). It is an intensity-based registration constraint. The third term is a registration constraint which ensures that energy minima map Ω_1 onto Ω_0. It is defined on a region $\Omega - \phi(\Omega_1)$ which is an expected background of I^0. The function $S(y^2)$ is low when y is likely to be a background grey-level value and high when it is not. Due to the third term, the registration model also enables the segmentation of an otherwise unknown region of interest in I^0. After minimization, boundaries of this region of interest are described by $\phi(\partial\Omega_1)$.

It can be shown using Green's formulae that Problem 1 is equivalent to the following problem [4, 5]:

Problem 1 (equivalent formulation) *Find an element of $\mathcal{W} \times \mathcal{C}$ which minimizes an energy J which is of the following form:*

$$J(u,g) = \frac{1}{2}\, A_{\Omega_1}(u,u) + \frac{\gamma_1}{2} |I^0_{\phi,g} - I^1|^2_{\Omega_1} - \gamma_2 \int_{\Omega_1} S((I^0_\phi(x))^2) \det(\nabla\phi)\, dx, \quad (6)$$

with free boundary conditions on $\partial\Omega_1$.

In this equation, the real value $\det(\nabla\phi)$ is the Jacobian of ϕ. In this formulation, contrast changes g are explicitly mentioned as unknown variables.

2.3 Numerical Solution

The gradient $\nabla J_{u,g}$ of the energy J (Equation (6)) with respect to the variable u in $\mathcal{W}$ was computed in [5, 4]. It is given by

$$\nabla J_{u,g} = u - L^{-1}\, f(\phi, g), \quad (7)$$

where L is the operator of the linearized elasticity [5, 4] and f is given by

$$\begin{aligned} f(\phi,g) = &-\gamma_1\, (I^0_{\phi,g} - I^1)\, \nabla I^0_\phi \\ &+2\,\gamma_2\, \det(\nabla\phi)\, S'((I^0_\phi)^2)\, \nabla I^0_\phi - \gamma_2\, \mathrm{div}\{S((I^0_\phi)^2)\, \mathrm{cof}(\nabla\phi)^T\}, \end{aligned} \quad (8)$$

where $\mathrm{cof}(M)$ is the cofactor matrix of a matrix M ($\mathrm{cof}(M) = \det(M) M^{-T}$).

Now, let u be fixed in $\mathcal{W}$, the function G_u which is defined on $\mathbb{R}^2$ and associates g to $J(u,g)$ is convex. Thus, the minimum of G_u is the unique solution of Euler equations $\partial_{g_1} G_u(g) = 0$ and $\partial_{g_2} G_u(g) = 0$, where $\partial_{g_1} G_u(g)$ and $\partial_{g_2} G_u(g)$ are respective partial derivatives of G_u:

$$\partial_{g_1} G_u(g) = \gamma_1 \big(g_1 \int_{\Omega_1} (I^0_\phi(x))^2 dx + g_2 \int_{\Omega_1} I^0_\phi(x) dx - \int_{\Omega_1} I^1(x) I^0_\phi(x) dx \big),$$

$$\partial_{g_2} G_u(g) = \gamma_1 \big(g_1 \int_{\Omega_1} I^0_\phi(x) dx + g_2 |\Omega_1| - \int_{\Omega_1} I^1(x) dx \big),$$

The solution $\hat{g}_u$ of the Euler equations is given by:

$$\hat{g}_{1,u} = \frac{\int_{\Omega_1} I^1(x)\, I^0_\phi(x) dx - \int_{\Omega_1} I^1(x) dx \int_{\Omega_1} I^0_\phi(x) dx}{\int_{\Omega_1} (I^0_\phi(x))^2 dx - (\int_{\Omega_1} I^0_\phi(x) dx)^2}, \tag{9}$$

$$\hat{g}_{2,u} = \frac{1}{|\Omega_1|} (\int_{\Omega_1} I^1(x) dx - \hat{g}_1 \int_{\Omega_1} I^0_\phi(x) dx). \tag{10}$$

Using these remarks, we can derive a gradient descent algorithm for the numerical resolution of Problem 1.

Algorithm 1 (gradient descent)

$$\forall\, t > 0, \quad \frac{du}{dt}(t) = -u(t) + \delta(t) \quad \text{and} \quad u(0) = M_0, \tag{11}$$

where at each time t, $\delta(t)$ is the solution of the following partial differential equation:

$$L\, \delta = f(\phi(t), \hat{g}(t)), \tag{12}$$

with f defined as in Equation (8) and $\hat{g}(t)$ given by Equations (9) and (10) for $u = u(t)$.

For the implementation of this algorithm, we use the same approach as in [4, 5]: we discretize Equation (12) using the Galerkin method and adopt a multigrid, coarse-to-fine optimization strategy. Also, the initial segmentation of the region of interest in I^0 is computed with the same approach. An initial displacement, M_0, is derived using a coarse matching of regions of interest boundaries.

3 Mammogram Model

Evaluation of the image registration problem was performed using synthetic mammograms based upon an anthropomorphic breast model and a simulation of the mammographic imaging process developed by P. Bakic et al. [12]. The 3D anthropomorphic breast model has been designed with a realistic distribution of large and medium scale tissue structures. Parameters controlling the size and placement of the simulated structures (adipose compartments and ducts) provide a method of consistently modeling images of the same simulated breast with different compression, projection angle and acquisition parameters. The mammographic imaging process is simulated using a compression model and a model of the x-ray image acquisition process. This mammography simulation has been evaluated in terms of mammographic texture [13] and ductal morphology [19], and has been used to estimate the mean glandular dose in mammography [20]. The compression model estimates breast deformation using published values of tissue elasticity parameters and clinically relevant force values. Synthetic mammograms are simulated using a monoenergetic parallel x-ray beam applied to the synthetically compressed breast phantom.

3.1 3D Anthropomorphic Breast Model

The breast model contains two ellipsoidal regions of large scale tissue elements: predominantly adipose tissue (AT) and predominantly fibroglandular tissue (FGT). Analysis of subgross histologic breast images and the corresponding mammograms showed that the background texture, or parenchymal pattern, found in mammograms is predominantly due to the projection of the connective tissue surrounding adipose compartments. These compartments are included in the model to simulate the breast adipose tissue, and these form the medium scale breast model elements. In addition, the model includes a representation of the breast ductal network. The adipose compartments are approximated by thin shells in the AT region and small blobs in the FGT region. The interiors of the shells and blobs have the elastic and x-ray attenuation properties of adipose tissue; while the shell layer and the portion of the FGT region surrounding blobs simulate the properties of the connective tissue. As a first approximation, the adipose compartments are represented by spheres. The size of the spheres can vary to allow for normal breast anatomic variations. depending upon the amount of adipose tissue in the breast. Adipose compartments are more easily identified in a histology image than in a mammogram, since the latter image contains the superimposed projections of many tissue layers. Generation of the simulated adipose compartments is described in more detail in [12] and generation of the binary tree models of the breast ductal networks is given in [19].

3.2 Simulation of Mammographic Compression

Mammographic compression is simulated based upon tissue elasticity properties and a simplified breast deformation model. Deformation is simulated separately for slices of the breast model positioned normal to the compression plates. Each slice is approximated by a beam composed of two different tissues. The deformed slices are stacked to produce a model of the compressed breast.

Tissue elasticity parameters from the literature vary significantly, partly because they have been measured experimentally using small samples taken from a particular tissue type. The breast, however, consists of a complex admixture of different tissues types, which affects the elastic behavior of the whole organ. We used parameters calculated from the speed of sound in tissue [21] and tissue density. The Mammography Quality Standards Act [22] recommends the minimum and maximum compression force to be used in mammography. There are also reports in literature of statistical analyses of the force and compressed breast thickness measured during exams [23]. The values of the force used in the mammographic simulation were selected based upon these two constraints.

In this paper we have generated medio-lateral oblique (MLO) mammographic views calculated with various amounts of compression. The breast compression simulation is performed in the following steps. First, a slice, with thickness equal to the desired image resolution (200 micron/pixel in this experiment) is approximated by a rectangle with total area and nipple-chest wall dimension equal as in the original slice. The FGT region within the slice is approximated by a rectangle which again has the same area and nipple-chest dimension as in the original slice. These approximations are designed

so that the distance between the centers of gravity of the whole slice and the FGT portion is also the same as in the original slice. Next, the rectangular approximation is deformed using Hooke's law and elastic moduli values corresponding to the FGT and the surrounding AT regions. Finally, the deformed rectangular approximation is used to compute the compressed phantom slice shape. Attention is taken to realistically simulate the flattened shape of the compressed breast. As such, the breast thickness is equal to the distance between the compression plates everywhere except in a narrow region close to the anterior edge of the breast. Separate processing of individual model slices is performed, followed by restacking the deformed slices together to form the 3-D compressed breast model. Computation details can be found in [12].

4 Results and Discussion

We have applied the modeling approach described in Section 3 to synthesize mammographic images of the same simulated breast under varying amounts of compression. Examples are shown on Figures 1(a) and (d). Varying breast compression has several effects on the appearance of the mammograms. The size of the breast domain in the mammogram increases as the breast becomes more compressed and the shape changes slightly. As the compression is varied, the FGT region, the central bright region composed of predominantly fibro-glandular tissue, also undergoes significant geometric deformations. As the compression decreases, the center of this region translates in the direction of the chest wall. The FGT region also changes its shape in a way that is indicative of a non-rigid deformation. Regions where fatty tissues are predominant also vary. In particular, in the top (simulated axilla) of images, the fatty tissue region which is between the FGT and the background becomes narrower as the compression decreases.

Compression variations affect the mammogram contrast. Increasing the amount of compression results in reducing the thickness and spreading the breast FGT region, which, if acquisition parameters remain constant, reduces the image latitude. Such a change can for instance be observed in Figure 2 by comparing histograms of mammograms obtained with different amount of compression. Note that the mammogram obtained with a compression of 8cm appears darker (lower pixel intensities) than the others (see Figure 1). This is because that mammogram was simulated with different acquisition parameters, which corresponds to a clinical situation of manually changing the x-ray technique for breasts of different thickness.

The algorithm described in Section 2 was applied to pairs of synthetic images, with the goal of correcting shape and intensity differences between structures in the unregistered mammograms. Parameter values were selected in accordance with our previous works [4, 5]. Computation times were about twenty seconds on a PC Intel Pentium IV 2.2 GH. A registration example is shown on Figure 1. In this example, the source image I^0 (image (a)) is the mammogram obtained with a breast compression of 8cm. It is deformed onto the target image I^1, which is the mammogram obtained with a breast compression of 5cm. Observing images (a), (b) and (d) and images (e) and (f), several significant corrections of geometric differences between mammogram coarse structures are noticeable. First of all, very few differences due to breast size variations remain after registration. These large differences are corrected as the result of a strong dilation

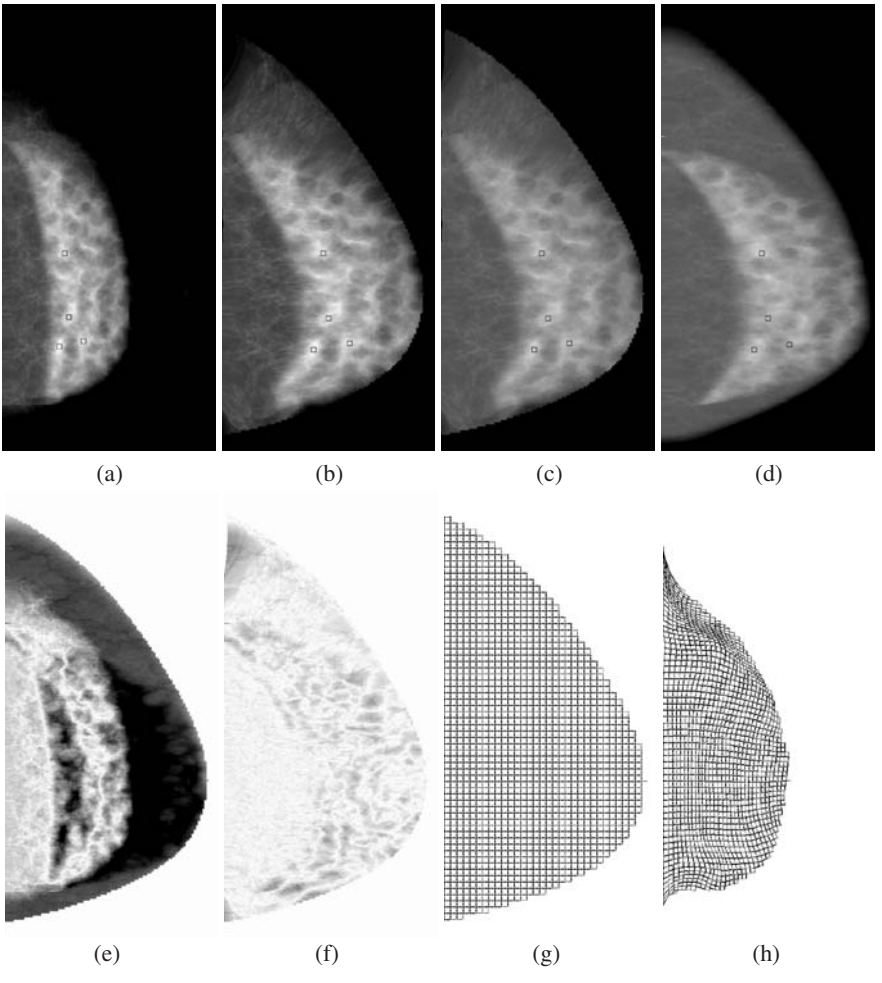

Fig. 1. A mammogram registration example: (a) and (d) are simulated mammograms of the breast with compressions of 8cm and 5cm, respectively. (a) is the source image I^0 and (d) is the target image I^1. (b) is the geometric deformation I^0_ϕ of I^0 that is computed using Algorithm 1. (c) is the contrast corrected deformation $I^0_{\phi,g}$ of I^0. [Small squares in (a), (b), and (d) indicate positions of several corresponding homologous salient points.] Absolute differences between unregistered mammograms (I^0 and I^1) and between registered and contrast corrected mammograms ($I^0_{\phi,g}$ and I^1) are shown respectively in (e) and (f) [black=high differences, white=low differences]. (g) shows the tessellated breast domain Ω_1 of I^1 and (h) the deformed domain ($\phi(\Omega_1)$).

of the source image. Initial differences due to variations in the shape of the FGT region are also significantly reduced. Left FGT boundaries in the source mammogram are particularly deformed. Their shape, which is approximately a straight line, is transformed into a curved line. In addition, in the upper portions of Figures 1(a) and (b), we can observe a large dilation of the source image which corrects shape differences of fatty tissue areas.

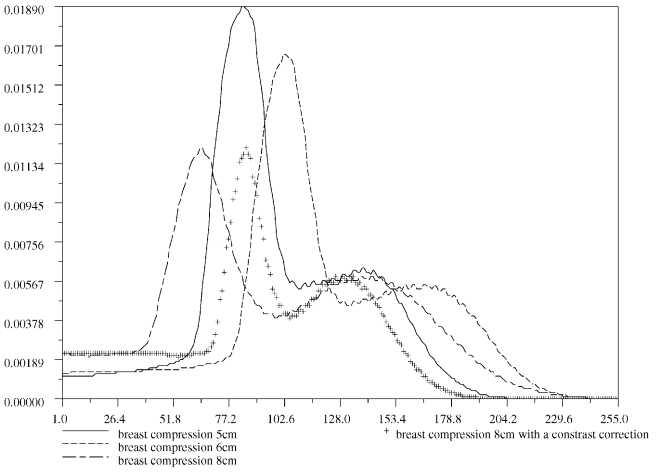

Fig. 2. Comparison of grey-level histograms of simulated mammograms.

The algorithm not only corrects coarse structure shapes. As can be seen in Figure 1(f), it also corrects some differences inside these structures. Such corrections can also be illustrated using salient points. In Figures 1(c) and (d), we selected manually four pairs of homologous salient points having the same positions and computed back their positions in Figure 1(a). The observed displacements of these points (marked with small squares) outline repositioning of homologous points of inner structures during the registration. The algorithm also provides for relevant correction of image contrast variations, as illustrated by Figure 1(c). This correction can also be seen in the comparison of mammogram histograms on Figure 2. As a result of the contrast change, histogram of the mammogram with a breast thickness of 8cm matches the histogram of the mammogram of thickness 5cm.

5 Conclusions

We have described a non-rigid mammogram registration algorithm, modified to provide corrections for image contrast variations. Use of the proposed algorithm was demonstrated on synthetic mammograms generated by applying different amounts of mammographic compression to the same 3D software breast phantom. Further studies are needed, aimed at more precise statistical evaluation of the algorithm.

References

1. J. Maintz and M.A. Viergever. A survey of medical image registration. *Medical Image Analysis*, 2(1):1–36, 1998.
2. U. Grenander and M.I. Miller. Computational Anatomy: an emerging discipline. *Quarterly of Applied Mathematics*, 56(4):617–694, December 1998.
3. A. Toga. *Brain mapping*. Academic Press, 1999.

4. F. Richard and L. Cohen. A new image registration technique with free boundary constraints: application to mammography. In A. Heyden et al., editor, *Proc. ECCV*, volume 4, pages 531–545, Copenhaguen, Denmark, may 2002. Springer.
5. F. Richard and L. Cohen. Non-rigid image registration with free boundary constraints: application to mammography. *Journal of Computer Vision and Image Understanding, Special issue on Nonrigid registration*, 89(2-3):166–196, 2003.
6. F. Richard and C. Graffigne. An image-matching model for the registration of temporal or bilateral mammogram pairs. In M. Yaffe, editor, *Proc. of the 5th International Workshop on Digital Mammography*, pages 756–762, Toronto, Canada, June 2000. Medical Physics.
7. M.Y. Sallam and K. Bowyer. Registration and difference analysis of corresponding mammogram images. *Medical Image Analysis*, 3(2):103–118, 1999.
8. J.L. Semmlow, A. Shadagopappan, L.V. Ackerman, et al. A fully automated system for screening Xeromammograms. *Computers and Biomedical Research*, 13:350–362, 1980.
9. R.P. Highnam and J.M. Brady. *Mammographic image analysis*. Kluwer series in Medical Imaging. Kluwer Academic Publishers, Dordrecht; Boston, March 1999.
10. R. Novak. *Transformation of the female breast during compression at mammography with special reference to importance for localization of a lesion.* PhD thesis, Departement of Diagnostic Radiology at Lakarhuset and Karolinska Sjukhuset, Sweden, 1989.
11. P. Bakic, D. Brzakovic, P. Brzakovic, et al. An approach to using a generalized breast model to segment digital mammograms. In *Proc. of 11th IEEE Symposium on Computer-Based Medical Systems*, pages 84–89, Lubbock, 1998.
12. P. Bakic, M. Albert, D. Brzakovic, and A. Maidment. Mammogram synthesis using a 3D simulation. i. breast tissue model and image acquisition simulation. *Medical Physics*, 29(9):2131–2139, 2002.
13. P. Bakic, M. Albert, D. Brzakovic, and A. Maidment. Mammogram synthesis using a 3D simulation. ii. evaluation of synthetic mammogram texture. *Medical Physics*, 29(9):2140–2151, 2002.
14. F. Maes, A. Collignon, D. Vandermeulen, et al. Multi-modality volume registration by maximization of mutual information. *IEEE Trans. on Medical Imaging*, 16(2):187–198, 1997.
15. P. Viola and W. Wells. Alignment by maximization of mutual information. *Intern. J. of Comp. Vision*, 24(2):137–154, 1997.
16. Y. Amit. A non-linear variational problem for image matching. *SIAM Journal on Scientific Computing*, 15(1):207–224, January 1994.
17. R. Bajcsy and S. Kovacic. Multiresolution elastic matching. *CVGIP*, 46:1–21, 1989.
18. G.E. Christensen, R.D. Rabbitt, and M.I. Miller. Mathematical textbook of deformable neuroanatomies. In *Proc. Natl. Acad. Sci., USA*, volume 90, pages 11944–11948, dec 93.
19. P. Bakic, M. Albert, and A. Maidment. Classification of galactograms using ramification matrices: preliminary results. *Academic Radiology*, 10(2):198–204, 2003.
20. R. Hunt, D. Dance, P. Bakic, et al. Monte carlo simulation of x-ray mammography using a realistic voxel phantom. In *Proc. of UK Radiological Congress*, Birmingham, UK, 2003.
21. G. Kossoff, E.K. Fry, and J. Jellins. Average velocity of ultrasound in the human female breast. *J. Acoust. Soc. Amer.*, 53:1730–1736, 1973.
22. ACR Committee on Quality Assurance in Mammography. *Mammography Quality Control Manual*. Amercan College of radiology, Reston, VA, 1999.
23. D. Sullivan, C. Beam, S. Goodman, and D. Watt. Measurement of force applied during mammography. *Radiology*, 181:355–357, 1991.